Resonant Raman scattering at exciton states tuned by pressure and temperature in 2*H*-MoS_2

Tsachi Livneh* and Eran Sterer
Department of Physics, Nuclear Research Center, Negev, P.O. Box 9001, Beer-Sheva 84190, Israel
(Received 1 April 2009; revised manuscript received 8 December 2009; published 18 May 2010)

We report on the temperature and pressure dependence of Stokes and anti-Stokes Raman spectra of a single crystal of 2*H*-MoS_2 as the energies of the A_1 and B_1 excitons, E_{A1} and E_{B1}, are tuned to resonate with an exciting laser at E_L=1.96 eV. Pressure- and temperature-dependent intensity ratio analysis of the resonant A_{1g} phonon and the E^1_{2g} phonon is complemented by the calculation of resonance Raman probability profiles of the former, which well agree with experiments. The temperature-dependent proximity of E_{A1} and E_{B1} to E_L is reflected in the formation of Stokes dominated A_1 and anti-Stokes dominated B_1 temperature "zones" with a midpoint positioned at $T\sim 260$ K. The shift in the frequency of the Stokes two-phonon dispersive band relative to that of the anti-Stokes band is explained as due to changing in the order of participation of the quasiacoustic phonon in the scattering process.

DOI: 10.1103/PhysRevB.81.195209 PACS number(s): 78.30.−j, 71.20.Nr, 71.35.Gg

I. INTRODUCTION AND BACKGROUND

Resonance Raman scattering has been widely used to study electronic band structures and to investigate the nature of electron-phonon interactions in semiconductors.[1] A key issue in those studies is the role played by intermediate exciton states, which are usually explored by varying the incident photon energy across the interband transition energy.[2] Some studies use an alternative approach in which the exciton is tuned to resonate with the laser at a fixed energy, either by applying high hydrostatic pressure at a constant temperature,[3] or by varying the temperature at ambient pressure.[4] Below we present a study of both temperature and pressure dependence, which greatly differ in their effect on the shift of excitonic-transition energies and broadening parameters. Those are analyzed under a single framework and complemented by a calculated Stokes and anti-Stokes Raman probability profiles of the resonant A_{1g} phonon.

The studied system is a crystalline 2*H*-MoS_2, a transition-metal dichalcogenide layer-type indirect semiconductor.[5] 2*H*-MoS_2 exhibits direct transitions around 2 eV characterized by an *A*-*B* excitonic pair,[6] which correspond to the minimal direct gaps in the *K* point of the Brillouin zone ($K_4 \rightarrow K_5$ and $K_1 \rightarrow K_5$ for the *A* and *B* excitons, respectively[7]). The separation between the energies of the *A* and *B* excitons is due to interlayer interaction and spin-orbit splitting.[7]

Limits on the use of excitons concern their lifetime and binding energy. Exciton lifetimes may restrict the distance they can travel. In temperature-dependent studies the binding energy restricts the temperature of operation since shallow binding causes the exciton to split under thermal fluctuations.[1] However, one has to bear in mind that short lifetime may cause excitonic features to vanish, even if the binding energy is relatively high.

The quasi-two-dimensional nature of the crystal structure enhances the binding energies of the *A*-*B* excitonic pair.[5] The relatively broad stability range of the excitons as a function of temperature and pressure makes this system attractive for a study of the correlation between the temperature- and pressure-dependent resonant Raman scattering.

The Raman spectra of bulk 2*H*-MoS_2 have been studied under ambient[8,9] as well as under high hydrostatic pressure.[10,11] No systematic study has yet been performed on the temperature dependence of the Raman spectrum. A group-theoretical analysis of the optical lattice vibrations[8] reveals four Raman-active modes corresponding to the following symmetries with measured frequencies under ambient conditions: E^2_{2g} (32 cm^{-1}), E_{1g} (286 cm^{-1}), E^1_{2g} (383 cm^{-1}), and A_{1g} (408 cm^{-1}). In addition, there are two IR active modes: E^2_{1u} (384 cm^{-1}), A_{2u} (470 cm^{-1}), and four silent modes: B^2_{2g}, E_{2u} (287 cm^{-1}), B_{1u} (403 cm^{-1}),[12] and B^1_{2g} (470 cm^{-1}). Resonant Raman spectra have previously been reported using tunable laser energies near the absorption edge.[2,12] Those spectra have been analyzed in terms of both first-order zone-center and higher-order Raman scattering. Some of the modes are enhanced by the coupling of phonon modes to electronic transitions associated with excitonic states.[9,12]

Calculations of the dynamic electronic band structure in bulk 2*H*-MoS_2 (Ref. 9) show that when "applying" the A_{1g} mode to a single layer of MoS_2, both the direct and indirect gaps are strongly modulated. In contrast, the E^1_{2g} mode couples only weakly to the electronic structure. Comparison of the dependence of the Raman cross section of the A_{1g} and E^1_{2g} phonons on the excitation laser energy[2] reveals two peaks centered at about the energy of the A_1 and B_1 excitons for both phonons. However, the cross section of the former is more than one order of magnitude larger than the latter.

The different coupling of the A_{1g} and E^1_{2g} phonons can be explained by the different directions of atomic displacements in the unit cell. In 2*H*-MoS_2 the character of the K_5 final state of the direct electronic transition is associated with the d_{z^2} orbitals of the Mo ion.[7] Those orbitals are pointed perpendicular to the atomic planes. Displacements of atoms in that direction as in the A_{1g} mode will strongly affect the polarizability while displacements of atoms in the parallel direction as in the E^1_{2g} mode has only a minor effect.[9]

In order to study the Raman spectra over a wide range of pressure and temperature a detailed knowledge of the dielectric properties of the bulk is necessary. If not available, a measure of the resonance Raman cross section is obtained by "normalizing" the scattering intensity of the resonant A_{1g} mode to the E^1_{2g} intensity. While both are similarly affected

by the bulk dielectric properties, the A_{1g} mode is much more sensitive to resonant effects and is treated as described above.

The stability of the A_1 and B_1 excitons, with binding energies of 42 and 134 meV,[7] is limited by pressure. Upon increasing pressure the excitons stability is reduced due to the increased number of free carriers.[13] Conductivity increases[14,15] until a critical value is reached, where exciton formation is no more possible. At $T=300$ K the binding energy of A_1 excitons decreases under pressure at a rate of ~ 7 meV/GPa.[13] As a consequence A_1 excitons dissociate when pressures are higher than ~ 6 GPa.

An increase in temperature reduces the stability of excitons.[5] This causes the excitation of electrons into the conduction band, until the excitons will dissociate.[5] There are as yet no absorption/reflectivity data for $T>300$ K from which we can determine the temperature dependence of the energies and stability range of the excitons. However, as we will show below, this issue can be clarified by analyzing the resonant behavior of the system.

II. EXPERIMENT

Raman spectra were measured in backscattering configuration using a Jobin-Yvon LabRam spectrometer with a He-Ne 632.8 nm laser (1.96 eV), which is slightly shifted from the energy of the A_1 exciton.[5] The scattered light was dispersed on a 1800 grooves/mm grating resulting in a ~ 1 cm^{-1} spectral resolution. Temperature-dependent spectra were measured by means of a Linkam continuously cooled liquid-nitrogen unit with a THMS600 stage plate. Laser-induced heating effects, which are due to the electronic resonance, were evaluated and care was taken to minimize them.

In order to measure pressure-dependent Raman scattering, a 30 μm single crystal 2H-MoS_2 flake was inserted in a Tel-Aviv-type diamond-anvil cell.[16] Three different sets of measurements were taken: in experiment no. 1 solid Ar was serving as a pressure-transmitting medium and Raman Stokes scattering spectra were measured up to 31 GPa. In experiments no. 2 and 3 a 1:4 ethanol-methanol liquid was the pressure-transmitting medium. Stokes and anti-Stokes spectra were measured in small pressure steps up to 7.1 GPa. The former was measured for increasing pressure and the latter for decreasing pressure. In all three experiments pressure was measured by the Ruby luminescence method.[17]

III. EXPERIMENTAL RESULTS

A. Effect of temperature on the Raman spectra

Figures 1(a) and 1(b) show anti-Stokes and Stokes Raman spectra for bulk 2H-MoS_2 measured at $T=95-573$ K. Here and in the following, a measure of the resonance Raman cross section is obtained by normalizing the scattering intensity of the resonant A_{1g} mode by the E^1_{2g} intensity. In addition to those two Raman allowed modes, the Raman inactive B_{1u} and E^2_{1u} phonons are also observed due to the resonant effect. The latter phonons are the Davydov couples of the former.[8] Three additional bands are marked "a," "b" (Ref. 12), and "c." The assignment of a (separated at low temperatures into two bands, "a_1"and "a_2") will be reported in a separate paper.[18]

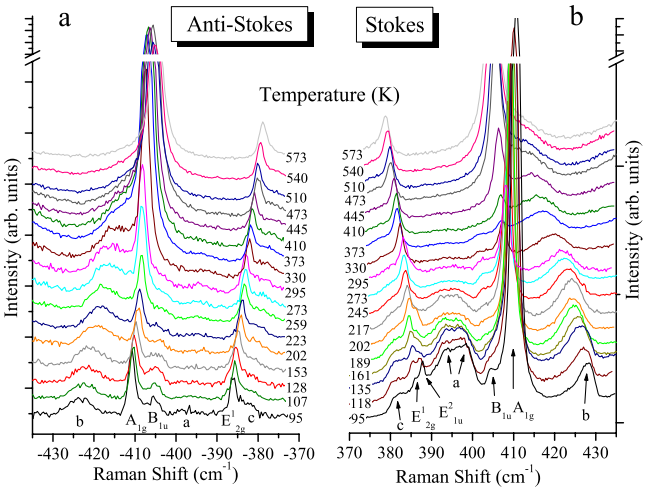

FIG. 1. (Color online) (a) Anti-Stokes and (b) Stokes and spectra for bulk 2H-MoS_2 measured at $T=95-573$ K and ambient pressure.

The Stokes scattering of the b band has been attributed to a two-phonon Raman process of successive emission of a dispersive quasiacoustic (QA) phonon and a dispersionless transverse-optical (TO) phonon. Both propagate along the c axis.[12] To explain the magnitude of the frequency $\omega_b=\omega_{QA}+\omega_{TO}$, the QA phonon was assigned to the Δ_2 branch (ending in the B^2_{2g} silent mode at the Γ point) and the TO phonon with finite wave vector in the vicinity of the Γ point (with E^2_{1u} symmetry) of the Δ_6 branch. The latter phonon (c phonon in this study) has been located at the lower-frequency side of the E^1_{2g} phonon [we note that reflectivity measurements locate the $E^2_{1u}(\Gamma)$ phonon on the high-frequency side of the $E^1_{2g}(\Gamma)$ phonon[8]].

Figure 2 compares the Stokes and anti-Stokes scattering on a crystal at $T=217$ K; unlike the other bands, the anti-

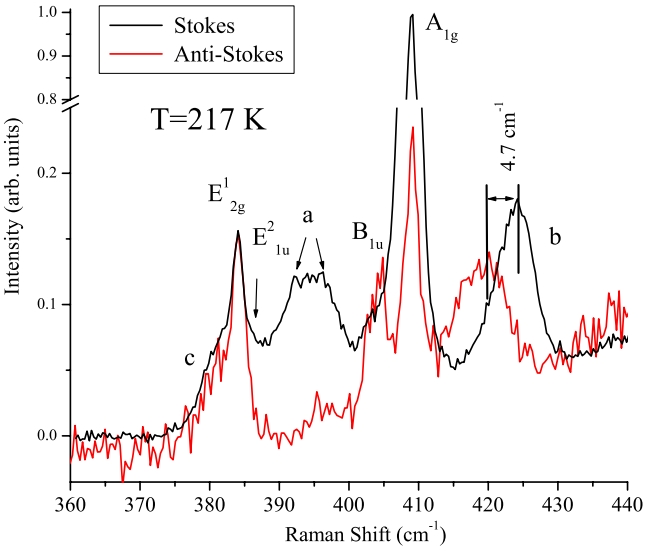

FIG. 2. (Color online) Stokes and anti-Stokes Raman scattering at $T=217$ K in the vicinity of the b band.

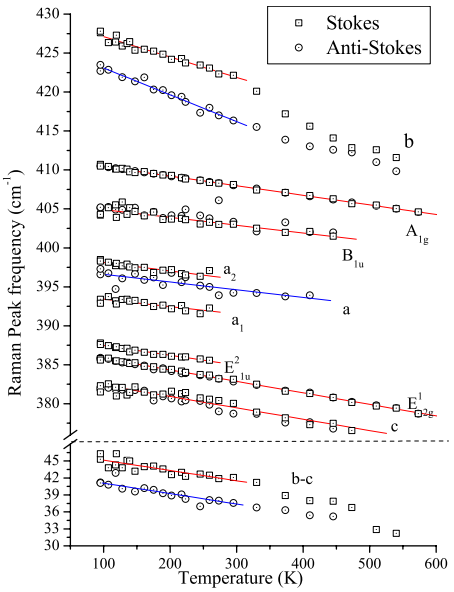

FIG. 3. (Color online) Temperature dependence of the peak positions of Stokes and anti-Stokes Raman scattering of $2H$-MoS_2 under ambient pressure.

Stokes and Stokes peak b band frequencies, ω_b^{AS} and ω_b^{S}, are shifted by ~ 4.7 cm^{-1}. This observation will be discussed below in Sec. IV C.

The temperature dependence of the Stokes and anti-Stokes peak frequencies has been obtained by a Lorentzian line-fitting procedure and is displayed in Fig. 3. The absolute values of the temperature coefficients $(\partial\omega/\partial T)_{P=0}$ of nearly all bands are seen from Table I to be roughly within $1.0-1.6\times10^{-2}$ cm^{-1}/K. In contrast, the temperature coefficients of the b band are significantly higher. This is due to the fact that the frequency shift of the latter is significantly affected by the change in the position of the exciton energy

TABLE I. Raman frequencies and pressure and temperature coefficients of the Stokes bands, and anti-Stokes (AS) bands when specifically noted, of $2H$-MoS_2.

Band	ω_0 (cm^{-1}) ($P=0$, $T=298$ K)	$(\partial\omega/\partial T)_{P=0}$ $\times10^{-2}$ (cm^{-1}/K)	$(\partial\omega/\partial P)_{T=298}$ (cm^{-1}/GPa)
c	380.0	−1.46(20)	
E^1_{2g}	383.1	−1.47(5)	1.80
E^2_{1u}	384.7	−1.26(12)	2.75
a_1	391.5	−0.96(30)	
a_2	396.0	−1.08(26)	
a	394.5	−0.99(33) (AS)	2.72
B_{1u}	402.9	−1.00(20)	2.23
A_{1g}	408.2	−1.23(5)	3.60
		($T\leq300$ K)	
b	422.2	−2.66(27)	3.8(4)
b (AS)	416.5	−3.44(32)	4.0(4)
(b-c)	42.1	−1.82(50)	
(b-c) (AS)	37.4	−1.72(20)	

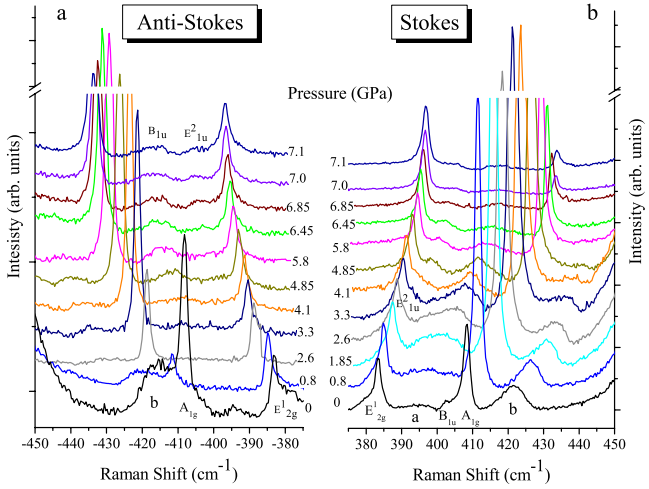

FIG. 4. (Color online) (a) Anti-Stokes and (b) Stokes Raman spectra for bulk $2H$-MoS_2 measured at $P\leq7.1$ GPa (experiment no. 3) and ambient temperature.

with respect to the excitation laser energy. The above add to phononic effects, which are related to strain dependence of the force constant. In the lower part of Fig. 3 we display the temperature dependence of the b band after subtracting that of the c band. It represents the net contribution of the QA phonon in the b band.

B. Effect of pressure on the Raman spectra

Figure 4 shows (a) anti-Stokes and (b) Stokes Raman spectra for bulk $2H$-MoS_2 measured at room temperature and for $P\leq7.1$ GPa (experiment no. 3). With the exception of the c band, all bands that have been found in the temperature-dependent study (Fig. 1) are also resolved in pressure-dependent spectra.

In a recent x-ray study of bulk $2H$-MoS_2 (Ref. 19) a discontinuity in the a and c unit-cell parameters has been found between pressures of 20.5 and 28.9 GPa. It has been suggested that such discontinuities are due to either an electronic or a structural phase transition with a small distortion of the $2H$ hexagonal structure. In order to find a signature for those processes, the pressure range has been extended to 31 GPa (experiment no. 1) (Fig. 5). A new band ("d" band) is seen to emerge above ~19 GPa on the higher-frequency side of the E^1_{2g} band. We also observe in the spectra a previously assigned and discussed band, marked as "e" in this study.[9]

Figure 6 displays the pressure dependence of the frequencies of the various bands. The frequencies were obtained by a Lorentzian line-fitting procedure. The inset of Fig. 6 shows the anti-Stokes and Stokes peak frequencies of the b band. Similarly to the temperature-dependent study, the peak frequencies of the former are redshifted with respect to the latter.

In Table I we show the pressure coefficients of the detected bands in experiments no. 1–3. In the first two the peak frequencies result from a linear regression fit. In experiment no. 1 those result from a least-square fit in the form $\omega(P)=\omega_0[(\delta_0/\delta')P+1]^{\delta'}$.[20] Derivation of this equation assumes

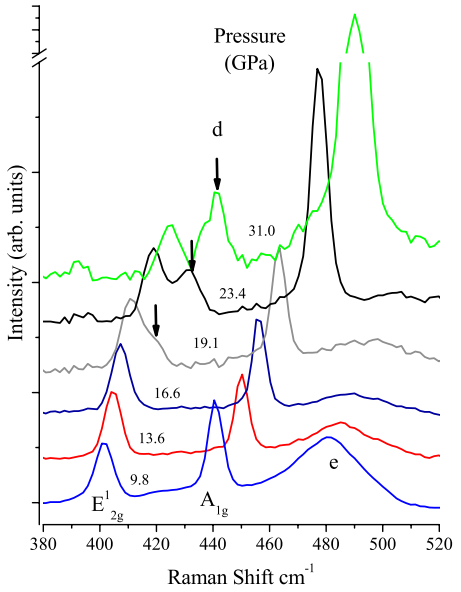

FIG. 5. (Color online) Stokes Raman spectra for bulk 2*H*-MoS_2 measured up to 31 GPa and ambient temperatures in experiment no. 1.

that the logarithmic pressure derivative δ of the frequency ω, varies linearly with pressure, $\delta=\delta_0+\delta' P$, where δ_0 is $(d \ln \omega/dP)_{P=0}$ and δ' is the pressure derivative of $d \ln \omega/dP$. The related frequency shift from experiment no. 1 is given in Table I corresponds to $\omega_0\delta_0$. Our pressure coefficients of the E^1_{2g} and A_{1g} phonons are in good agreement

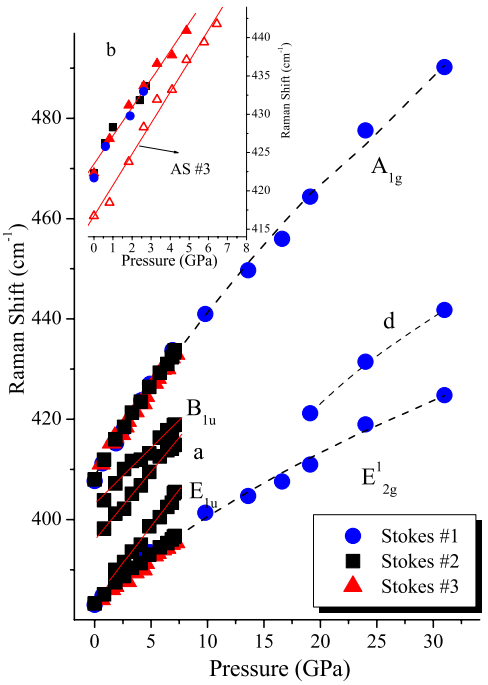

FIG. 6. (Color online) Pressure-dependent Stokes and anti-Stokes peak positions of 2*H*-MoS_2 under ambient temperature in experiments no. 1–3. In the inset: the respective peak frequencies of the b band.

with previous studies: Sugai[10] found pressure coefficients of 1.9 and 4.0 cm^{-1}/GPa, and Bagnall *et al.*[11] obtained 1.8 and 3.7 cm^{-1}/GPa.

IV. ANALYSIS AND DISCUSSION

In this section we compare experimental and calculated resonance Raman probability profiles which are strongly affected by the temperature and pressure dependence of the excitons energies. First, we discuss the identification of the intermediated exciton states which play a role in the resonant Stokes (anti-Stokes) Raman scattering process. Next, we discuss the indirectly evaluation of the temperature at which the B_1 exciton "loses" its stability. Finally, we discuss the assignment of the b band and a possible origin to the red frequency shift between the anti-Stokes and Stokes Raman scattering.

A. Resonance Raman probability profiles

The Raman scattering probability of a phonon (ph) in a vicinity of an 1*s* exciton state is[21]

$$P_{\rm ph} \approx (2\pi/\hbar) \left| \frac{\langle 0|H_{eR}(\omega_L)|1\rangle\langle 1|H_{e\text{-}ion}|1\rangle\langle 1|H_{eR}(\omega_s)|0\rangle}{(E_i-\hbar\omega_L-i\Gamma_1)(E_i-\hbar\omega_s-i\Gamma_1)} \right|^2. \quad (1)$$

Above H_{eR} and $H_{e\text{-}ion}$ are electron-radiation and electron-phonon interaction Hamiltonians, and 0 and 1 are the ground and the *i*th excitonic levels ($i=A_1,B_1$). ω_L and ω_s are the incident laser and scattered photon frequencies. The cases $E_i=\hbar\omega_L$ and $E_i=\hbar\omega_s$ are referred to as incoming and as outgoing resonances with E_i the energies of either the A_1 or B_1 exciton. The outgoing resonance in the AS and S A_{1g} modes occurs at one phonon energy below and above the exciton energy, i.e., at $E_i-\hbar\ \omega_{A1g}$ and $E_i+\hbar\ \omega_{A1g}$. The resonant scattering probabilities in those two cases are denoted by $P^{\rm AS}_{A1g}$ and $P^{\rm S}_{A1g}$. A measure of the Raman cross section is obtained by normalizing the scattering intensity of the resonant A_{1g} mode to the E^1_{2g} intensity.

The temperature dependence of the energies of the A_1 and B_1 excitons contain the Bose-Einstein occupation factor for the phonon and are given by[22]

$$E_i(T) = E_{iP0} - a_{iP}\left[1+\frac{2}{\exp(\Theta_{iP}/T)-1}\right]. \quad (2)$$

Above a_{iP} represents the strength of the electron (exciton)-phonon interaction and Θ_{iP} is the average phonon temperature. For $T\leq 300$ K the previously found E_{iP0}, a_{iP}, and Θ_{iP} are for A_1: 1.976 eV, 46 meV, and 220 K and for B_1: 2.179 eV, 42 meV, and 200 K [note that $E_i(0)\approx E_{iP0}-a_{iP}$ for $T\rightarrow 0$].[22]

For semiconductors the dependence of the broadening parameter Γ on temperature is[23]

$$\Gamma(T) = \Gamma_0 + \frac{\Gamma_{\rm LO}}{\exp(\Theta_{\rm LO}/T)-1}. \quad (3)$$

Above the width Γ_0 originates from temperature-independent mechanisms. $\Gamma_{\rm LO}$ is a measure of the strength of electron (exciton)-longitudinal-optical (LO) phonon interactions

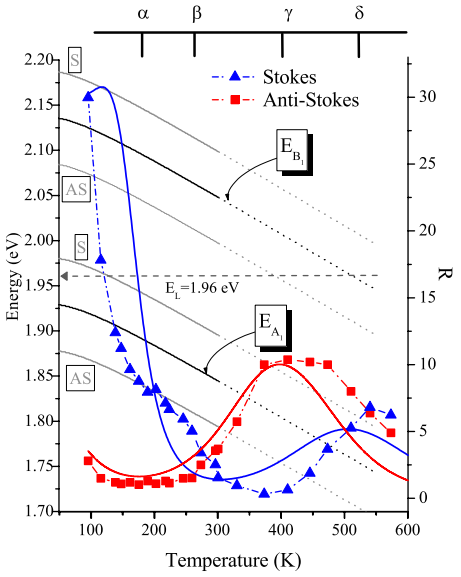

FIG. 7. (Color online) The effect of tuning E_i ($i=A_1,B_1$) on the resonance Raman scattering by changing the temperature. The left-hand scale refers to E_i (Ref. 22) and to the energies where the outgoing resonance in the AS and S A_{1g} modes occurs, i.e., $E_i-\hbar\,\omega_{A1g}$ and $E_i+\hbar\,\omega_{A1g}$. Those are shown as black and gray lines, respectively, for $T\leq 300$ K and as dotted lines for extended fits out to $T=550$ K. The right-hand scale $R=I_{A1g}/I_{E12g}$ is for Stokes (triangles), R^{S}, and anti-Stokes scattering (squares), R^{AS}. The calculated P^{S}_{A1g} and P^{AS}_{A1g} [Eq. (1)], are shown as blue and red solid lines. In the upper part, $\alpha-\delta$ divide the temperature scale into zones, which reflect the effect of the proximity of $E_L=1.96$ eV to the energy of the A_1/B_1 excitons and to their S/AS shifted energies.

while Θ_{LO} is the LO phonon temperature. Ho *et al.*[22] have measured $\Gamma(T)$ for A_1 and B_1 excitons and fitted their experimental data using Eq. (3) up to 300 K with Γ_{LO}, Θ_{LO} values of 75 meV and 560 K, and $\Gamma_0=18.0$ and 37.4 meV for, respectively, the A_1 and B_1 excitons.

The values of Θ_{LO} are quite close to previously reported LO phonon temperatures for $2H$-MoS_2 (557 K) obtained from Raman measurements.[8] This indicates that the variation in the broadening parameter of the A_1 and B_1 excitons, Γ, with temperature is mainly due to interaction of electrons with optical phonons.[22] According to Eq. (3) the exciton broadening increases with temperature above ~200 K at a rate of $\sim 10^{-4}$ eV/K.

Figure 7 shows the effect of tuning the energies of the A_1 and B_1 excitons on the resonance Raman excitation profile by changing the temperature. The intensity ratio $R=I_{A1g}/I_{E12g}$ for both S (R^{S}) and AS (R^{AS}) scattering, are shown as filled triangles and squares. Using the temperature dependence of the excitons energies and lifetime broadenings, Eq. (1) provides P^{AS}_{A1g} and P^{S}_{A1g}, which are shown as solid lines. The calculated fits have been obtained with the low-temperature values of E_{A1} and E_{B1} as reported in Ref. 12.[24] The numerators in Eq. (1) are assumed to be temperature independent and for the best fit to the measured R^{AS} and R^{S} the value for the B_1 exciton is 2.5 times that of the one for the A_1 exciton. Good agreement[26] is found between the profiles of the calculated P^{AS}_{A1g} and P^{S}_{A1g}, and the experimental R^{AS} and R^{S}.

Figure 7 also shows the temperature dependence of the energies of the A_1 and B_1 excitons and their A_{1g} phonon shifted energies, $E_i-\hbar\,\omega_{A1g}$ and $E_i+\hbar\,\omega_{A1g}$ for $T\leq 300$ K. The latter are for the outgoing resonance in the AS and S A_{1g} modes, respectively. The temperature shift of excitonic-transition energies is due to both the lattice-constant variations and interactions with acoustic and optical phonons. Since the latter holds for a wide temperature range, one may extend the temperature dependence of the parameter fit for the two exciton energies to higher temperatures (dotted lines). Those are used in Eq. (1) in order to obtain P^{AS}_{A1g} and P^{S}_{A1g} in the extended temperature range. The reasonable agreement of the latter with the data justifies the extended fit and motivates future exploration of the absorption and reflectivity characteristics of $2H$-MoS_2 at $T>300$ K.

Since $E_L=1.96$ eV lies between E_{A1} and $E_{A1}+\hbar\,\omega_{A1g}$, the ratio R^{S} is maximal for $T\approx 95$ K, when both incoming and outgoing resonances contribute to the Stokes cross section of the A_{1g} phonon. For $T>175$ K (marked as α on the upper horizontal scale) E_{A1} is detuned from E_L, and E_{B1} approaches E_L, with a midpoint (β) at ~260 K. This marks the boundary between the A_1 and the B_1 "zones." In that temperature range resonance effects are due to the proximity of E_L to the energy of both excitons or their Stokes/anti-Stokes shifted energies. R^{S} has a minimum around 350 K, while R^{AS} reaches a maximum at ~400 K (γ), since $E_L\approx E_{B1}-\omega_{A1g}$. For increasing temperature, the S signal rises while AS decreases. Finally, for $T\approx 520$ K (δ) the ratio of the S and AS A_{1g} intensities are represented by nonresonant $\exp(-\hbar\omega_{A1g}/kT)$ dependence, see discussion below.

Figure 8 shows the effect of tuning the A_1 exciton on the resonance Raman excitation profile by changing the pressure. The pressure dependence of E_{A1} (~0.02 eV/GPa), $E_{A1}-\hbar\,\omega_{A1g}$ and $E_{A1}+\hbar\,\omega_{A1g}$ as well as of R^{S} and R^{AS} is depicted. Its effect on the Stokes and anti-Stokes profiles significantly differs. At low pressure R^{S} increases with pressure up to ~3.8 GPa since it is closer in energy to E_L. R^{AS} first decreases as E_L is detuned from $E_{B1}-\hbar\,\omega_{A1g}$ (not shown) and then increases. For increasing pressures R^{S} is detuned from resonance whereas R^{AS} is becoming dominant below ~5 GPa. However, around this value the A_1 exciton becomes unstable[13] and the system can no more resonate with the excitation laser at $E_L=1.96$ eV.

The inset of Fig. 8 shows R^{S} (P) for experiment no. 1 at $P>10$ GPa, which extends beyond the stability range of the A_1 exciton. The increase in R^{S} with pressure is attributed to induced changes in the electronic band structure which enhances the interaction with the A_{1g} phonons. This point needs further investigation.

The pressure dependence $\Gamma_{A1}(P)\approx 35+3P$ (Γ_{A1} in meV) of the lifetime broadening of the A_1 exciton has been extracted from Fig. 4 of Ref. 13. We now use the pressure dependence of E_{A1} in order to employ Eq. (1) for the calculation of P^{S}_{A1g} and P^{AS}_{A1g}. Those are shown in Fig. 8 as solid lines.[25] The incoming and outgoing resonant peaks coalesce with decreasing exciton lifetime.[1] Since the shift in the peak position for increased pressures is significantly higher for E_{A1} than for $\hbar\,\omega_{A1g}$ the resonance is expected to peak at $P_m=[E_L-E_{A1}(0)\pm\frac{\hbar\omega_{A1g}(0)}{2}]/(\frac{\partial E_{A1}}{\partial P})_{300}$, i.e., ~3.8 and

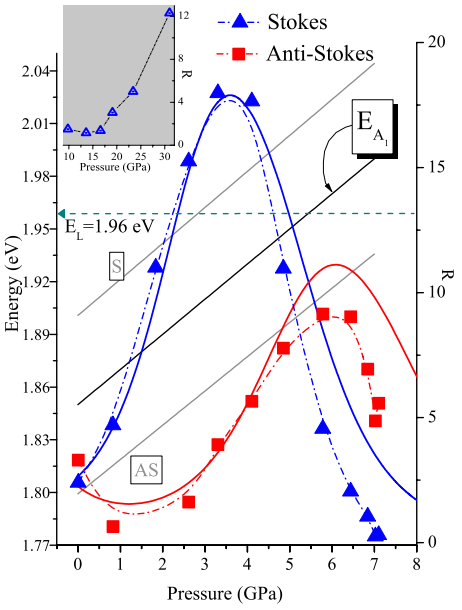

FIG. 8. (Color online) The effect of tuning E_{A1} on the resonance Raman scattering by changing the pressure (experiment no. 3). The left-hand scale refers to E_{A1} (Ref. 13) and the energies of the outgoing resonance in the AS and S A_{1g} modes. Those are depicted as black and gray lines, respectively. The right-hand scale refers to R^{S} (triangles) and R^{AS} (squares). The calculated pressure-dependent P^{S}_{A1g} and P^{AS}_{A1g} [Eq. (1)], are shown as blue and red solid lines. In the inset: R^{S} (P) for experiment no. 1 at $P>10$ GPa.

~6.3 GPa for the Stokes and anti-Stokes branches. P^{S}_{A1g} agrees with the measured R^{S} while P^{AS}_{A1g} deviates from R^{AS} for $P>5$ GPa. The latter is consistent with the A_1 exciton becoming unstable above ~6 GPa.[13]

B. Indirect evaluation of the B_1 exciton stability range

Figure 9 shows the measured temperature dependence of the ratio of anti-Stokes and the Stokes intensities of the A_{1g} $(I^{AS}_{A1g}/I^{S}_{A1g})$ and E^{1}_{2g} $(I^{AS}_{E2g}/I^{S}_{E2g})$ phonons, as well as the com-

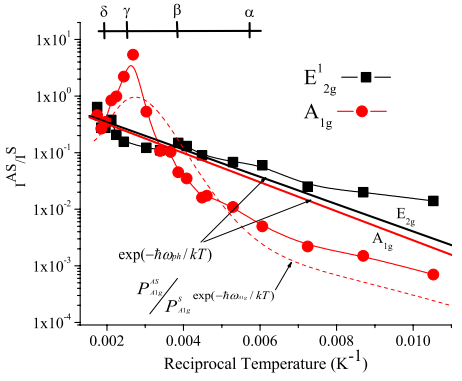

FIG. 9. (Color online) Temperature dependence of I^{AS}/I^{S} of the A_{1g} (circles) and E^{1}_{2g} (squares) phonons is compared to the temperature dependence of their Bose-Einstein factor. P^{AS}_{A1g}/P^{S}_{A1g} from Eq. (1) is also shown as dashed line, after being normalized by $n(\omega_{ph})/[n(\omega_{ph})+1]$. In the upper part, $\alpha-\delta$ divide the temperature scale into zones, as depicted in Fig. 7.

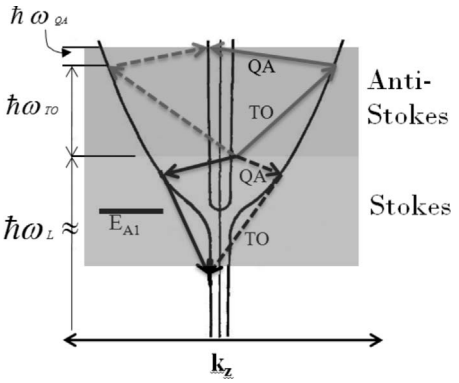

FIG. 10. Schematic representation of the two-phonon Raman scattering of polaritons by a longitudinal QA phonon and a TO dispersionless along the c axis. The Stokes scheme is from Ref. 12 and the anti-Stokes scheme is the addition due to our proposed mechanism. The dashed and solid lines show the α and β processes.

puted ratio P^{AS}_{A1g}/P^{S}_{A1g} from Eq. (1) (dashed line). The latter is normalized by $n(\omega_{ph})/[n(\omega_{ph})+1]$, where $n(\omega_{ph})=[\exp(\omega_{ph}/kT)-1]^{-1}$ is the Bose-Einstein factor for phonon energy $\hbar\omega_{ph}$. The temperature-dependent profiles of $(P^{AS}_{A1g}/P^{S}_{A1g})$ and $(I^{AS}_{A1g}/I^{S}_{A1g})$ are generally consistent.

For temperatures up to 175 K (marked by α on the upper scale) the I^{AS}/I^{S} ratios for the two phonons continue to differ by about an order of magnitude, which reflects the much stronger resonant nature of the A_{1g}, relative to the E^{1}_{2g} mode.[2] Two opposite effects dominate I^{AS}/I^{S}: increase in the Boltzmann factor and detuning of $E_{A1}+\hbar\omega_{A1g}$ from E_L.

For $T>175$ K, $E_{A1}+\hbar\omega_{A1g}$ shifts away from E_L. I^{AS}_{A1g}/I^{S}_{A1g} increases while I^{AS}_{E2g}/I^{S}_{E2g} follows the $\exp(-\hbar\omega_{E2g}/kT)$ dependence. Around $T\approx 260$ K (point β), I^{AS}_{A1g}/I^{S}_{A1g} intercepts the $\exp(-\hbar\omega_{A1g}/kT)$ line. It increases as $E_{B1}-\hbar\omega_{A1g}$ approaches E_L and reaches a maximum at $T\approx 400$ K (γ). Further increasing the temperature results in a decrease in I^{AS}_{A1g}/I^{S}_{A1g} and at $T\approx 520$ K (δ) the ratio recovers the $\exp(-\hbar\omega_{A1g}/kT)$ dependence.

We suggest that as long as the temperature dependence of I^{AS}_{A1g}/I^{S}_{A1g} follows the expected resonant profile, the B_1 exciton can be regarded as stable. Between 510 and 540 K this ratio reaches the $\exp(-\hbar\omega_{A1g}/kT)$ temperature dependence and we therefore consider the B_1 exciton to be stable up to ~520 K.

C. Dispersive Raman band

In a previous resonance Raman scattering study of Stokes scattering at $T=7$ K on a single crystal of $2H$-MoS_2 it has been shown that if the exciting laser line is above the $1s$ level of the A_1 exciton, a new band (b) appears at $\omega_b=429$ cm^{-1} and shifts toward lower frequencies while approaching the frequency of the A_{1g} phonon.[12] The Stokes peak in that band has been interpreted (see black lines in Fig. 10) in terms of a two-phonon process. In it a polariton in the inner branch, created in the crystal by an incident photon, is scattered to the outer branch by emitting a longitudinal QA phonon with a large wave vector parallel to the c axis. Then it is scattered by emitting a TO phonon (which is taken to be dispersionless

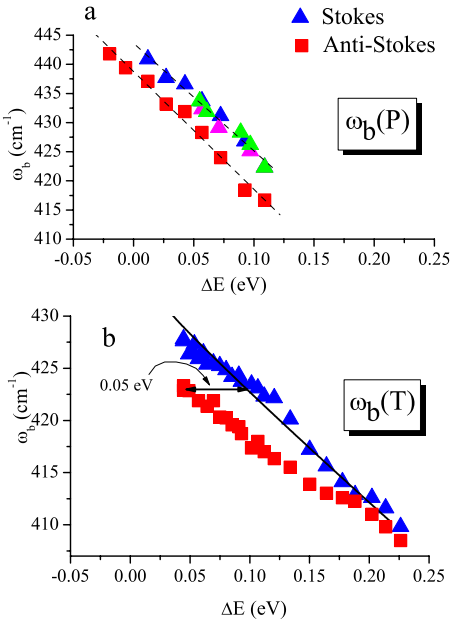

FIG. 11. (Color online) The (a) pressure and (b) temperature dependence of ω_b^{S} (triangles) and ω_b^{AS} (squares) as function of $\Delta E = E_L - E_{A1}$. The fit for temperature-dependent ω_b^{S} is shown by a solid line according to Eq. (4) (Ref. 12).

along Γ-A) into the photonlike polariton final state. As discussed above, the QA has been assigned to the Δ_2 branch and the TO phonon to a phonon from the Δ_6 branch with a finite wave vector.

The shift of ω_b is caused by a combination of phononic effects, related with strain dependence of the force constant, and by the change in the energy of the exciton with respect to the excitation laser energy. Using the temperature and pressure dependence of E_{A1} from Refs. 13 and 22, Fig. 11 displays the (a) pressure and (b) temperature dependence of ω_b^{S} and ω_b^{AS} as a function of $\Delta E = E_L - E_{A1}$. In both cases ω_b^{AS} is red shifted relative to the corresponding ω_b^{S}.

The dependence of ω_b^{S} on E_L has been modeled in Ref. 12. We use the same approach and set of parameters to model the dependence of ω_b^{S} on the temperature-dependent ΔE according to

$$\hbar\omega_b(q_z,T) = \Delta E(T) - \hbar^2\left(|q_z| \pm \omega_L\frac{n_0}{c}\right)^2/2M_{\mathrm{II}}^{A_1} + \hbar\omega_{\mathrm{TO}}(T). \tag{4}$$

q_z and k_z are the wave vectors of the QA phonon and the A_1 exciton along the c axis, M_{II}^{A1} is the sum of the effective masses of the electron and the hole, n_0 is the ordinary refractive index. The ± signs relate to the α process and β processes in Fig. 10.

The shift of the Stokes b peak have been fitted using a single fitted parameter, $\hbar\omega_{\mathrm{QA}}(0,300) = 52.4\ \mathrm{cm}^{-1}$ and the result is a solid line in Fig. 11(b). The energy of the QA phonon is in good agreement with the value 56 cm^{-1} from neutron inelastic scattering data.[27]

In Fig. 12 we compare the ΔE dependence of ω_b^{S}, which has been obtained by tuning E_L across E_{A1} at 7 K,[12] with that

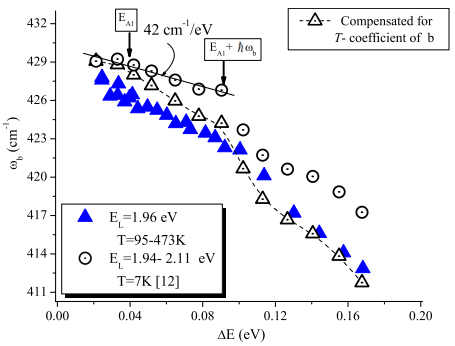

FIG. 12. (Color online) Comparison of the ΔE dependence of ω_b^{S}, obtained by tuning E_L across E_{A1} (at 7 K) (Ref. 12) (empty circles) with that obtained by tuning $E_{A1}(T)$ across E_L (at 1.96 eV) (full triangles). Empty triangles show the latter, after taking into account the temperature coefficient of the b mode.

from tuning $E_{A1}(T)$ across E_L at 1.96 eV. After inclusion of the effect of the temperature coefficient of the b band (Table I) the two signals reasonably agree. In both cases, the data do not show the predicted linear dependence over the entire ΔE range.[12] Separating $\Delta E \lesssim 0.11$ eV, the two regimes differ in their $(\frac{\partial\omega_b}{\partial\Delta E})$. We note that the "kinks" in both studies are found around the energy where the cross section of the dispersive b band is peaked at $E_{A1} + \hbar\,\omega_b$ (see Fig. 4 in Ref. 12). Taking $\omega_{\mathrm{QA}} = \omega_b - \omega_c$ we restrict our analysis of the QA phonon temperature coefficient to $\Delta E \leq 0.11$ eV where $(\frac{\partial\omega_{\mathrm{QA}}}{\partial T})_{P=0} = (\frac{\partial\omega_{\mathrm{QA}}^{\mathrm{ph}}}{\partial T})_{P=0} + (\frac{\partial\omega_{\mathrm{QA}}^{Ex}}{\partial T})_{P=0} \approx -1.82\times10^{-2}\ \mathrm{cm}^{-1}/\mathrm{K}$. The first and second terms on the right are the contribution to the temperature-dependent frequency shifts from shifts of the phonon and the exciton energies, respectively. Since $(\frac{\partial\omega_b}{\partial\Delta E})_{P=0}^{T=7} = -(\frac{\partial\omega_{\mathrm{QA}}}{\partial E_{A1}})_{P=0}^{T=7} \approx -42\ \mathrm{cm}^{-1}/\mathrm{eV}$ (Ref. 12) and $(\frac{\partial E_{A1}}{\partial T})_{P=0} = -(\frac{\partial\Delta E}{\partial T})_{P=0} \approx -3.8\times10^{-4}$ eV/K (Ref. 22) we find $(\frac{\partial\omega_{\mathrm{QA}}^{Ex}}{\partial T})_{P=0} = (\frac{\partial\omega_{\mathrm{QA}}}{\partial E_{A1}})_{P=0}^{T=7} \times (\frac{\partial E_{A1}}{\partial T})_{P=0} \approx -1.6\times10^{-2}\ \mathrm{cm}^{-1}/\mathrm{K}$ and therefore $(\frac{\partial\omega_{\mathrm{QA}}^{\mathrm{ph}}}{\partial T})_{P=0} \approx -2\times10^{-3}\ \mathrm{cm}^{-1}/\mathrm{K}$. Hence, the relatively high-temperature coefficient of the b band is mostly attributed to the change in the energy of the exciton rather than to phononic effects.

With no reliable information on the pressure coefficient of the c mode, the corresponding data are difficult to interpret. However, if we use the pressure coefficient of the TO E_{2g}^1 phonon we find $(\frac{\partial\omega_{\mathrm{QA}}}{\partial P})_{T=300} = (\frac{\partial\omega_{\mathrm{QA}}^{\mathrm{ph}}}{\partial P})_{T=300} + (\frac{\partial\omega_{\mathrm{QA}}^{Ex}}{\partial P})_{T=300} \approx 2.1\ \mathrm{cm}^{-1}/\mathrm{GPa}$. Since $(\frac{\partial E_{A1}}{\partial P})_{T=300} \approx 0.02$ eV/GPa,[13] $(\frac{\partial\omega_{\mathrm{QA}}^{Ex}}{\partial P})_{T=300} \approx 0.84\ \mathrm{cm}^{-1}/\mathrm{GPa}$, and $(\frac{\partial\omega_{\mathrm{QA}}^{\mathrm{ph}}}{\partial P})_{T=300} \approx 1.26\ \mathrm{cm}^{-1}/\mathrm{GPa}$. The significantly larger phononic contribution in the pressure-dependent shift of ω_{QA} compared to the temperature-dependent case is mostly attributed to the fact that temperature is more subtle than pressure in altering the interatomic spacings.[28]

The energy shift of the intermediate exciton state for $\omega_b^{\mathrm{AS}} = \omega_b^{\mathrm{S}}$ corresponds to the shift between the Stokes and the anti-Stokes curves in Fig. 11. This ~0.05 eV shift for $\Delta E \leq 0.11$ eV is close to the energy of the c mode.[29] We may therefore as follows explain the shift between ω_b^{AS} and ω_b^{S}: a polariton in the inner branch is scattered to the outer branch by absorbing a TO phonon and then it is scattered by absorb-

ing a QA optical phonon into the photonlike polariton final state. Hence, the Stokes and anti-Stokes processes are in reverse order; QA+TO for the Stokes and TO+QA for the anti-Stokes (see Fig. 10).

In the Stokes scattering spectra from $2H$-MoS_2, no switching on the order of the phonon emission as a function of E_L was found.[12] Such a phenomenon has been reported previously for the Stokes scattering of ZnTe (Ref. 30) and attributed to $\boldsymbol{q}$ dependence of matrix elements and from features in the density of states of intermediate excitons. The above proposed scheme is supported by the fact that anti-Stokes scattering are found in the pressure-dependent study at $\Delta E<0$, when no Stokes signal is detected; E_L is lower than E_{A1} but is sufficiently high for the initial position in the outer branch for the absorption of a QA phonon to be above E_{A1}; i.e., $E_L+\hbar\ \omega_{\mathrm{TO}}>E_{A1}$.

V. CONCLUSIONS

Raman-scattering spectra of $2H$-MoS_2 were measured at room temperature under hydrostatic pressures up to 31 GPa and under ambient pressure in the temperature range of $T=95-573$ K. The pressure and temperature dependence of the A_{1g} phonon scattering intensity, "normalized" by that of E^1_{2g}, well agrees with its calculated resonant Raman profile, as the A_1 and B_1 excitons are tuned to resonate with E_L of the exciting laser. The temperature-dependent proximity of E_{A1} and E_{B1} to E_L is reflected in the formation of Stokes dominated A_1 and anti-Stokes dominated B_1 temperature "zones." Information on the temperature and pressure range where excitons are stable is also provided by identifying the conditions at which the system is no longer resonant. From the temperature-dependent measurement, the B_1 exciton appears to be stable up to ~520 K. The ~0.05 eV shift in the frequency of the Stokes two-phonon dispersive b band relative to that of the anti-Stokes band is explained as due to changing in the order of participation of the quasiacoustic phonon in the scattering process.

ACKNOWLEDGMENTS

We thank Leila Zeiri from the chemistry department in Ben-Gurion University for assistance with acquiring the Raman spectra. We gratefully acknowledge Uri Banin for helpful discussions.

*Corresponding author; t.livneh@nrcn.org.il

[1] M. Cardona, in *Light Scattering in Solids II*, edited by M. Cardona and G. Güntherodt (Springer-Verlag, Berlin, 1983), p. 19.
[2] T. Sekine, T. Nakashizu, M. Izumi, K. Toyoda, K. Uchinokura, and E. Matsuura, J. Phys. Soc. Jpn., Suppl. A **49**, 551 (1980).
[3] I. H. Choi and P. Y. Yu, Phys. Rev. B **68**, 165339 (2003).
[4] N. M. Gasanly, A. Aydinli, and H. Özkan, Cryst. Res. Technol. **36**, 1393 (2001).
[5] J. A. Wilson and A. D. Yoffe, Adv. Phys. **18**, 193 (1969).
[6] B. L. Evans and P. A. Young, Proc. R. Soc. London, Ser. A **298**, 74 (1966).
[7] R. Coehoorn, C. Hass, and R. A. de Groot, Phys. Rev. B **35**, 6203 (1987).
[8] T. J. Wieting and J. L. Verble, Phys. Rev. B **3**, 4286 (1971).
[9] G. L. Frey, R. Tenne, M. J. Matthews, M. S. Dresselhaus, and G. Dresselhaus, Phys. Rev. B **60**, 2883 (1999).
[10] S. Sugai and T. Ueda, Phys. Rev. B **26**, 6554 (1982).
[11] A. G. Bagnall, W. Y. Liang, E. A. Marseglia, and B. Welber, Physica B **99**, 343 (1980).
[12] T. Sekine, K. Uchinokura, T. Nakashizu, E. Matsuura, and R. Yoshizaki, J. Phys. Soc. Jpn. **53**, 811 (1984).
[13] G. A. N. Connell, J. A. Wilson, and A. D. Yoffe, J. Phys. Chem. Solids **30**, 287 (1969).
[14] M. Dave, R. Vaida, S. G. Patel, and A. R. Jani, Bull. Mater. Sci. **27**, 213 (2004).
[15] A. W. Webb, J. L. Feldman, E. F. Skelton, L. C. Towle, C. Y. Liu, and I. L. Spain, J. Phys. Chem. Solids **37**, 329 (1976).
[16] E. Sterer, M. P. Pasternak, and R. D. Taylor, Rev. Sci. Instrum. **61**, 1117 (1990).
[17] H. K. Mao, J. Xu, and P. M. Bell, J. Geophys. Res. **91**, 4673 (1986).
[18] T. Livneh (unpublished).
[19] R. Aksoy, Y. Ma, E. Selvi, M. C. Chyu, A. Ertas, and A. White, J. Phys. Chem. Solids **67**, 1914 (2006).
[20] H. Hanfland, B. Beister, and K. Syassen, Phys. Rev. B **39**, 12598 (1989).
[21] P. Yu and M. Cardona, *Fundamentals of Semiconductors* (Springer-Verlag, Berlin, 1999), p. 393.
[22] C. H. Ho, C. S. Wu, Y. S. Huang, P. C. Liao, and K. K. Tiong, J. Phys.: Condens. Matter **10**, 9317 (1998).
[23] P. Lautenschlager, M. Garriga, S. Logothetidis, and M. Cardona, Phys. Rev. B **35**, 9174 (1987).
[24] There is a wide range of published values of low temperatures E_{A1} and E_{B1}, for which their choice will strongly affect the calculated profiles: 1.935 ± 0.05 eV and 2.142 ± 0.05 eV (Ref. 22), E_{A1} (7 K)=1.9449 eV and E_B (7 K)=2.1376 eV (Ref. 12) (recalling that below 15 K they are practically constant) and 1.9326 and 2.1295 eV at $T=77$ K (Ref. 6), which extrapolates at $T\rightarrow0$ to 1.942 and 2.142 eV. The calculated fit for Eq. (1) has been attained by using E_{A1} and E_B reported in Ref. 12. An outcome of this result is the attribution of room-temperature values of E_{A1} and E_B (1.85 and 2.02 eV), which are consistent with Ref. 22 and are different from the values that are generally cited in the literature [1.88 and 2.06 eV (Ref. 9)].
[25] For the pressure-dependent calculations we use $E_{A1}(300\ \mathrm{K})=1.85$ eV, which is consistent with Ref. 22.
[26] The "bend" in the R^S profile at ~170 K is attributed to a 30 meV shift of the I_{E2g} (E_L) peak with respect to I_{A1g} (E_L) (Ref. 2).
[27] N. Wakabayashi, H. G. Smith, and R. M. Nicklow, Phys. Rev. B **12**, 659 (1975).
[28] B. Weinstein and R. Zallen, in *Light Scattering in Solids IV*, edited by M. Cardona and G. Güntherodt (Springer-Verlag, Berlin, 1984), p. 515.

[29] For higher ΔE this shift decreases until it practically vanishes for $\Delta E(T) \approx 0.17$ eV with $T \sim 470$ K, which is close to the highest temperature where the A_1 exciton has been observed in the absorption spectra (Ref. 5). We attribute the decrease in the shift between the Stokes and anti-Stokes scattering to effects which are related with the broadening of the excitons to the extent that the analysis for $\Delta E \leq 0.11$ eV is not feasible. The same argument applies for the absence of the expected increase in ω_b^S as E_L "crosses" E_{B1} (Ref. 12).

[30] Y. Oka and M. Cardona, Solid State Commun. **30**, 447 (1979).